Available online at www.sciencedirect.com
ScienceDirect
Ceramics International 35 (2009) 2891–2897
CERAMICS INTERNATIONAL
www.elsevier.com/locate/ceramint

Fabrication and characterization of 1D brushite nanomaterials via sucrose ester reverse microemulsion

HongNgee Lim [a,*], Anuar Kassim [a], NayMing Huang [b], Rauzah Hashim [c], Shahidan Radiman [d], PoiSim Khiew [e], WeeSiong Chiu [e]

[a] Chemistry Department, Faculty of Science, Universiti Putra Malaysia, 43400 UPM Serdang, Selangor Darul Ehsan, Malaysia
[b] Physics Department, Faculty of Science, Universiti Malaya, 50603 Kuala Lumpur, Malaysia
[c] Chemistry Department, Faculty of Science, Universiti Malaya, 50603 Kuala Lumpur, Malaysia
[d] School of Applied Physics, Faculty of Science and Technology, University Kebangsaan Malaysia, 43000 Bandar Baru Bangi, Selangor Darul Ehsan, Malaysia
[e] Faculty of Engineering & Computer Science, Nottingham University, Jalan Broga, 43500 Semenyih, Selangor Darul Ehsan, Malaysia

Received 5 February 2009; received in revised form 23 February 2009; accepted 28 March 2009
Available online 24 April 2009

Abstract

In the present study, 1-dimensional (1D) brushite nanomaterials were fabricated through sucrose ester based reverse microemulsion for the first time. X-ray diffraction patterns revealed that the nanomaterials possessed brushite crystal phase with trace amount of hydroxyapatite. The size and morphology of brushite crystals were governed by the changes in the aqueous-to-sucrose ester weight ratio at low initial reactant concentration, giving rise to rod-like and fibre-like 1D nanomaterials. Brushite nanorods and nanofibres with average diameters of 25.53 ± 4.60 nm (aspect ratio ~ 6) and 76.18 ± 19.74 nm (aspect ratio ~ 40), respectively, had been synthesized. As the reactant concentration increased, it became the key factor in controlling nucleation and crystal growth, rendering the aqueous-to-sucrose ester ratio unimportant. Formation mechanism of various morphologies of brushite crystals is postulated.

Keywords: Calcium phosphates; Brushite; Sucrose ester; Microemulsion; Low dimensional nanomaterials

1. Introduction

Bone is a highly metabolically active tissue; remodelling continues throughout life. The remodelling process is an active coupling of the processes of bone formation and resorption [1] sustained by the regulated action of osteoclasts and osteoblasts [2]. Calcium phosphates constitute the major inorganic phase of bone, are bioactive and can be rapidly integrated into the human body [3,4]. Therefore, they are of high relevance to material science, biology and medicine.

Calcium orthophosphates are salts of tribasic phosphoric acid, H_3PO_4 and its ionic compounds. Hydroxyapatite $Ca_5(PO_4)_3(OH)$, octacalcium phosphate $Ca_8H_2(PO_4)_6{\cdot}5H_2O$, monetite $CaHPO_4{\cdot}2H_2O$, and brushite $CaHPO_4{\cdot}2H_2O$ are different crystalline orthophosphates that have been extensively studied for their relevance in biological mineralization [5]. Brushite has raised considerable interest amongst researchers in bone substitution due to their fast resorption as it is a metastable compound when used under physiological conditions [6–8]. The biocompatibility and degradation of brushite have been demonstrated in several in vitro and in vivo studies [9–11]. Following immersion in aqueous media, brushite may, depending on conditions, be stable, disintegrate or dissolve and precipitate as hydroxyapatite [12].

As the natural bone is made of calcium phosphate nanoparticles scattered in the organic matrix [13], it is believed that deliberate tailoring of the crystallite size, morphology, stoichiometry and composition of calcium phosphates could lead to improved properties such as bioactivity, biocompatibility, surface area, chemical and physical stability and mechanical properties by adjusting the concentration of reactants, concentration of surfactants, pH and temperature [14–16]. The different forms of particulate calcium phosphates manufactured and sold in the market include irregular

* Corresponding author. Tel.: +60 163301609; fax: +60 358911088.
E-mail address: janet_limhn@yahoo.com (H. Lim).

0272-8842/$36.00
doi:10.1016/j.ceramint.2009.03.044

multifaceted particles and smooth rounded particles, with solid or porous structure [17]. They are osteoconductive and help in growth and attachment of bone [18,19], and are clinically used in oral surgical procedures to augment the alveolar ridge [20] and in periodontal repair [21]. Kent et al. [22] reported improved denture stability and retention when dense calcium phosphate particles have been used for augmentation of atrophic mandibular and maxillary alveolar ridges.

Many researchers have explored fabrication of calcium phosphate nanoparticles of various morphologies such as lath [16], rod [23], belt [24], sheet, needle [25], wire [26], and cone [27]. Among the processing routes used to fabricate the nanoparticles are sol–gel [14], solid state [28], biosynthesis [29], chemical precipitation [5], hydrothermal [30,31], hard templating [23], emulsion [32,33] and microemulsion [16].

Reverse microemulsion is a well-known processing route in the fabrication of calcium phosphate nanoparticles. Surfactant stabilized discontinuous aqueous phase acts like a nanoreactor that can control nucleation and crystal growth in restricted geometries [34–36]. Surfactants that have been used to stabilize microemulsion for preparation of calcium phosphate nanoparticles are tricaprylmethylammonium chloride [16], sorbitan monooleate [25], polyoxyethylene sorbitan monooleate [37] and octaethylene glycol monododecyl ether [38].

In this paper, we utilized sucrose ester S1670 as nonionic food grade biosurfactant to form water-in-oil (w/o) reverse microemulsion (water/heptan-1-ol/sucrose ester) as a soft template for the synthesis of brushite crystals. To the best knowledge of the authors, no work has been reported using sucrose ester as biosurfactant in reverse microemulsion for the synthesis of brushite nanoparticles. These surfactants are biodegradable and formed from renewable resources such as fatty acids and sugars. In order to monitor changes in nucleation and crystal growth, reactant concentration and water-to-surfactant weight ratio (*W/S*) were considered. Based on the experimental results, plausible formation mechanism of the brushite crystals is discussed.

2. Experimental

2.1. Materials

The starting materials used in this work were calcium chloride dihydrate, $CaCl_2{\cdot}2H_2O$ (Sigma–Aldrich), disodium hydrogen phosphate, Na_2HPO_4 (Sigma–Aldrich), heptan-1-ol (Merck) and food grade sucrose ester (Mitsubishi-Kagaku Foods Corporation). The sucrose ester used in this work is a commercially available sucrose monoester of stearic acid (S1670, HLB = 16, at least 70% monoester of stearic acid) in a mixture of di-, tri- and polyesters of stearic acids. All reagents were of analytical grade and were used as received. Deionized water ($\geq$18.2 MΩ) was used throughout the study.

2.2. Fabrication of calcium phosphate crystals

Sucrose ester was mixed thoroughly with heptan-1-ol (sucrose ester-to-heptan-1-ol weight ratio equivalent to 0.80) using a vortex mixer. $CaCl_2{\cdot}2H_2O$ aqueous solution was added into the above mixture followed by Na_2HPO_4 aqueous solution under constant stirring with predetermined amount of aqueous-to-surfactant weight ratio (*W/S*) to form a transparent reverse microemulsion. The calcium-to-phosphate molar ratio is 1.67, similar to that of natural bone and teeth [39]. The microemulsions were aged at 40 °C for seven days. After aging, the microemulsions were demulsified with ethanol (98%, Fluka). The white precipitates were washed with ethanol and deionized water until they were free from organic matter. All the precipitates were calcined at 600°C for 2 h. The calcium phosphate crystals were prepared in reverse microemulsion containing *W/S* = 0.25, 0.40 and 0.60 with $CaCl_2{\cdot}2H_2O$:Na_2HPO_4 concentrations of (I) 0.10 M:0.06 M, (II) 0.30 M:0.18 M and (III) 0.50 M:0.30 M, respectively. Bulk calcium phosphate was prepared using conventional wet chemical processing route whereby 0.50 M $CaCl_2{\cdot}2H_2O$ aqueous solution was titrated with 0.30 M Na_2HPO_4 aqueous solution under constant stirring as a comparison to the reverse microemulsion-prepared calcium phosphates.

2.3. Characterization of calcium phosphate crystals

Crystallinity of the calcium phosphate powders was measured using a Phillips X-Ray Diffractometer (XRD). Measurements were taken from 15° to 70° on the 2θ scale at a size step of 0.033° s^{-1}. The Cu anode X-ray was operated at 40 kV and 30 mA in combination with a Ni filter to give monochromatic Cu Kα radiation at 1.54 Å. Qualitative analysis was performed with Xpert HighScore using the JCPDS PDF-2 database [40]. Chemical bonding of the powders was analyzed using a Perkin Elmer Fourier Transform Infrared (FTIR) spectroscopy. The powders were mixed with potassium bromate, ground homogenously and converted into pellets. The spectra (% transmittance with wavenumber) were recorded. Size and morphology of the powders were observed using a Phillips HMG 400 Transmission Electron Microscopy (TEM) under 100 kV accelerating voltage and a LEO 1455 Variable Pressure Scanning Electron Microscopy (SEM). Samples for TEM observation were dispersed in ethanol and sonicated for five minutes to avoid aggregations. The mixtures were then placed on carbon-coated 400 mesh copper grids and dried at room temperature overnight before examination. Samples for SEM observation were mounted on aluminum stubs using double-sided tape and vacuumed coated with gold in a Polaron SC500 sputter coater.

3. Results and discussion

Fig. 1 shows the XRD patterns of bulk (a) and reverse microemulsion-prepared calcium phosphates (b), which portrayed almost similar diffraction profiles. The diffraction peaks of the crystals are indexed to brushite crystal structure (JCPDS file no. 2-0085) with trace amount of hydroxyapatite. No characteristic peaks of other calcium phosphate phases and impurities are detected. The intensity of the diffraction peaks indicates that the samples were well crystallized. Low pH and

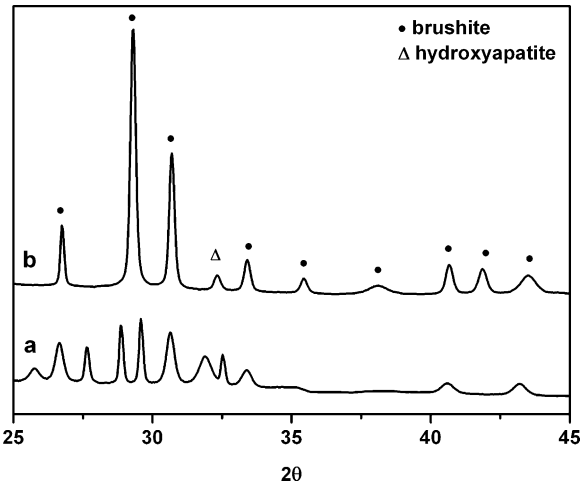

Fig. 1. XRD patterns of (a) bulk brushite and (b) brushite nanorods synthesized in reverse microemulsion with $W/S = 0.25$ at 0.10 M calcium and 0.06 M phosphate ions, respectively.

the absence of pH adjustment to above 6.5 on the sucrose ester reverse microemulsion for nucleation and crystal growth have rendered brushite the predominant phase [41]. Similar conditions with pH lower than 6.5 for the formation of brushite have also been reported [42–45]. This is because the consumption of phosphate ions in the formation and growth of brushite would reduce the pH of the solution due to the release of hydrogen ions from the HPO_4^{2-} dissociation [5]. It was found that the relative intensity at $2\theta = 29.5^\circ$ for the brushite crystals synthesized in the reverse microemulsion is higher than the standard. It is because of their preferential growth along a certain crystal plane due to constraint and prolate shape of the water droplets in the sucrose ester reverse microemulsion [46]. The result is consistent with the EM observation which shows morphologies of elongated particles.

Fig. 2(a) shows the FTIR spectra of the reverse microemulsion-prepared brushite crystals after calcination at 600 °C with $W/S = 0.25$ and reactant concentration of 0.1 M $CaCl_2{\cdot}2H_2O$ and 0.06 M Na_2HPO_4. The spectrum is free from alkyl group signifying the absence of residual organic materials. The broad band at 3000–3800 cm^{-1} was caused by stretching and bending of residual-free water. Additional band at 1600 cm^{-1} was attributed to bending mode of O–H group due to absorbed water. The weak band at 2900 cm^{-1} is assigned to O–H stretching of brushite [5]. Fig. 2(b) highlights the FTIR spectra of the brushite crystals with wavenumber from 400 to 1250 cm^{-1}. The spectrum exhibits easily distinguishable bands attributed to PO_4^{3-}. The bands in the range of 430–520 cm^{-1}, 520–630 cm^{-1} and 720 cm^{-1} were assigned to υ_2 O–P–O bending mode, υ_4 O–P–O bending mode and phosphate group bending mode, respectively [13,47]. The bands at 900–990 cm^{-1} and 990–1250 cm^{-1} were assigned to υ_1 symmetric P–O stretching mode and υ_3 antisymmetric P–O stretching mode, respectively [24]. The PO_4^{3-} bands extensive split at 1125 cm^{-1} suggests high crystallinity of the brushite crystals which is consistent with the XRD result.

Fig. 3 shows the TEM and SEM images of typical morphology of bulk brushite prepared using conventional wet chemical precipitation method. The bulk brushite consists of merged large planes forming irregular chunky material with dimension > 10 μm and high polydispersity due to the absence of templating system during preparation. In contrast, brushite crystals obtained through reverse microemulsion approach had smaller dimensions, unique morphologies and are well defined as depicted in the EM micrographs (Figs. 4–6). The size and morphology of the brushite crystals are controlled within the aqueous core of the reverse microemulsion.

The morphologies of the brushite crystals prepared with 0.10 M and 0.06 M of calcium and phosphate concentrations, respectively, were influenced by the W/S ratios as distinguished in the EM micrographs in Fig. 4. At $W/S = 0.25$, brushite nanorods with diameter 25.53 ± 4.60 nm and length ~150 nm were formed in the microemulsion (Fig. 4(a)) while for $W/S = 0.40$, brushite nanofibres with diameter 76.18 ± 19.74 nm and length ~2 μm were produced (Fig. 4(b)). The formation of

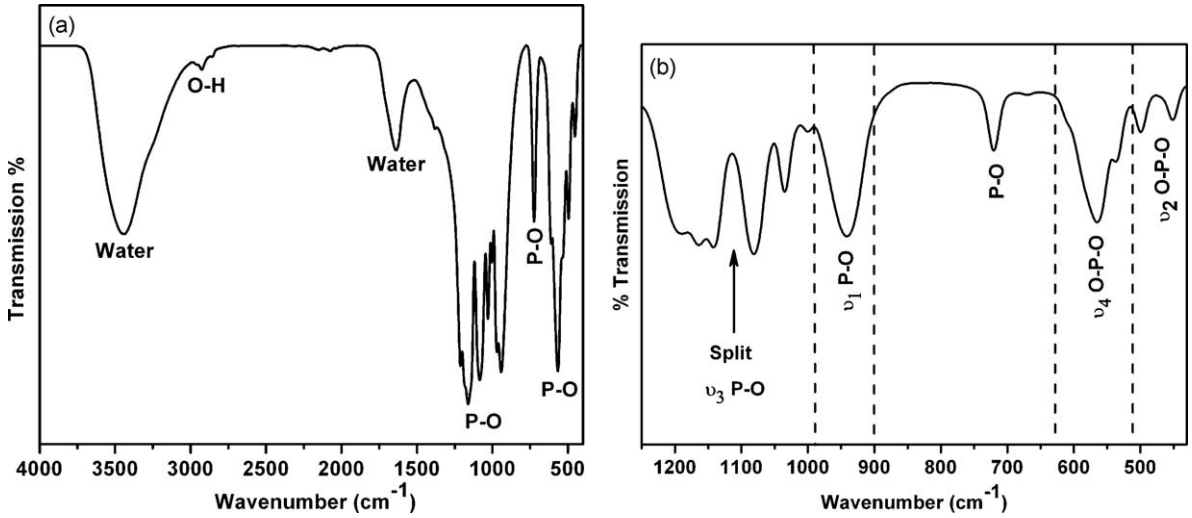

Fig. 2. FTIR spectra of (a) brushite and (b) highlights of chemical bonding of brushite synthesized in reverse microemulsion with $W/S = 0.25$ at 0.10 M calcium and 0.06 M phosphate ions, respectively.

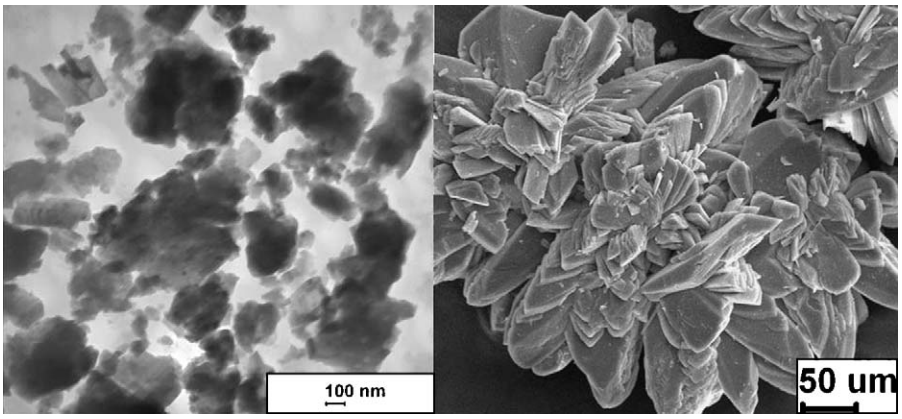

Fig. 3. TEM micrograph (left) and SEM micrograph (right) for bulk brushite.

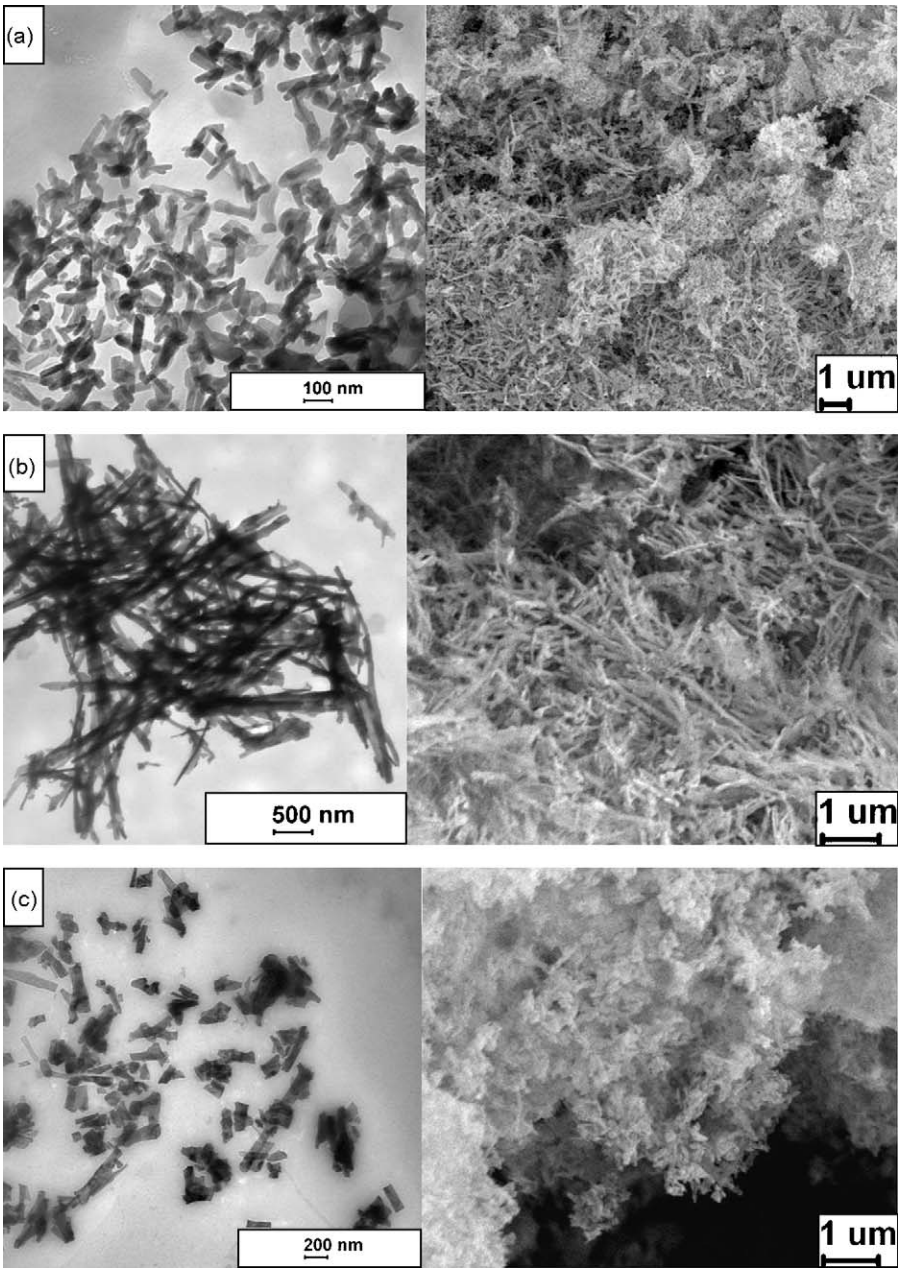

Fig. 4. TEM micrographs (left) and SEM micrographs (right) for (a) brushite nanorods, (b) brushite nanofibres and (c) lath-shaped brushite.

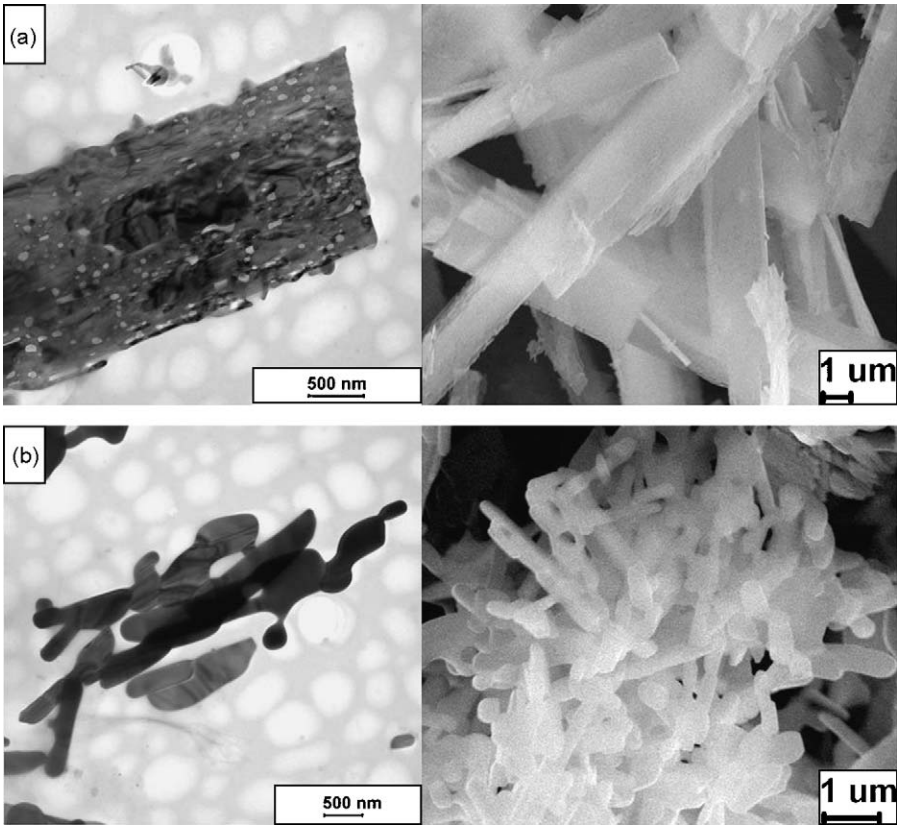

Fig. 5. TEM micrographs (left) and SEM micrographs (right) for (a) lath-shaped brushite and (b) branched rod-like brushite.

rod-like and fibre-like brushite nanomaterials is due to the confinement of the inorganic materials in the aqueous cores of sucrose ester microemulsion which have a prolate shape [46]. Furthermore, the low rate of brushite growth which is affected by the low reactant concentration [48] allows the confinement of brushite crystals in the water droplets of microemulsion. With higher *W/S* value, the length of the brushite particles became longer. At $W/S = 0.25$, aqueous droplets will have a shorter prolate shape and thus, the resulted nanomaterials will tend to have shorter 1D materials or nanorods with aspect ratio < 5. Increasing the water content will result in the formation of longer prolate aqueous droplets and thus, nanofibres with aspect ratio > 40 were formed. With high *W/S* value, 0.60, the brushite particles formed have irregular shape with lath-like morphology. This is because at high *W/S* value, the amount of water droplets is high and these water

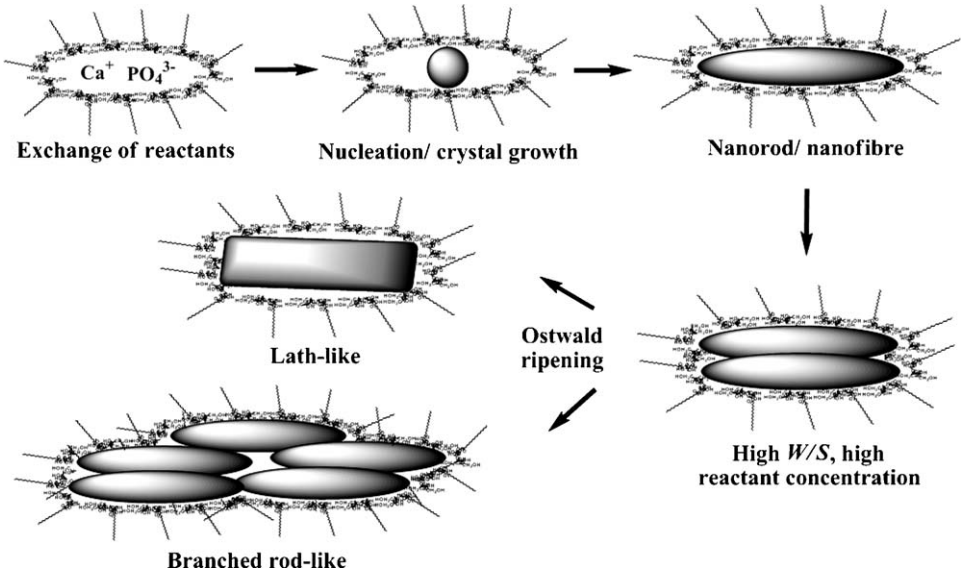

Fig. 6. Schematic of the brushite crystal growth within the aqueous core of sucrose ester microemulsion.

droplets are too close to each other which lead to the Ostwald ripening process as shown in Fig. 6.

From the schematic mechanism in Fig. 6, the aqueous droplets containing calcium and phosphate ions in the sucrose ester microemulsion will continuously collide with each other due to the Brownian motion. This will result in the fusion of the aqueous droplets and exchange of the reactants [49]. Then, nucleation and crystal growth happen in the aqueous droplets of the microemulsion. Upon aging, the particles grow larger and adopt the shape of the prolate water droplets. Further growth of the brushite crystals resulted in the formation of nanorods and nanofibres while lath-like particles formed with $W/S \geq 0.60$.

When concentration of calcium and phosphate ions are increased to 0.30 M and 0.18 M, effect of the *W/S* value did not significantly affect the size and morphology of the brushite crystals. It was found that all the brushite particles formed under $W/S = 0.25$, 0.40 and 0.60 exhibited lath shape with length and width of 15 μm and 2 μm, as shown in Fig. 5(a). For calcium and phosphate ions concentration of 0.50 M and 0.30 M, branched rod-like brushite particles were formed in the microemulsion system with $W/S = 0.25$, 0.40 and 0.60 as shown in Fig. 5(b). This observation is in agreement with previous studies that at high reactant concentration, crystal growth will lead to branched rod-like morphology [50,51]. The lath-like and branched rod-like morphologies are contributed by the Ostwald ripening process in the microemulsion. The schematic of crystal growth resulted from Ostwald ripening is shown in Fig. 6. At high reactant concentration, nucleation and crystal growth rate is higher and the produced crystals in the water cores tend to aggregate to form larger particles [49]. Under the influence of sucrose ester microemulsion, the aggregation leads to the formation of lath-like and branched rod-like brushite crystals.

4. Conclusion

Brushite particles with controllable size and morphology have been successfully fabricated using sucrose ester based reverse microemulsion as a soft template to regulate nucleation and crystal growth. Nanorods and nanofibres were formed at low *W/S* ratios (0.25 and 0.40) and low reactant concentration of 0.10 M Ca^{2+} and 0.06 M PO_4^{3+}. This observation underlines the significant influence of sucrose ester concentration on the final size and morphology of the nanoparticles. On the contrary, the brushite crystals possessed almost similar size and morphology regardless of the *W/S* ratio at ≥0.30 M Ca^{2+} and ≥0.18 M PO_4^{3+} where reactant concentration controlled nucleation and crystal growth. By tailoring reactant concentration at pre-determined *W/S* value, reverse microemulsion stabilized by sucrose ester provides a convenient and straight forward route for fabrication of various sizes and morphologies of brushite crystals for biomedical applications.

Acknowledgement

The author (HongNgee Lim) would like to thank Universiti Putra Malaysia for the award of Graduate Research Fellowship.

References

[1] D.J. Hunter, P.N. Sambrook, Bone loss: epidemiology of bone loss, Arthritis Research and Therapy 2 (2000) 441–445.
[2] G.C. Babis, P.N. Soucacos, Bone scaffolds: the role of mechanical stability and instrumentation, Injury 36S (2005) S38–S44.
[3] L.L. Hench, Bioceramics: from concept to clinic, Journal of the American Ceramic Society 74 (1991) 1487–1510.
[4] S. Weiner, H.D. Wagner, The material bone: structure-mechanical function relations, Annual Review of Materials Science 28 (1998) 271–298.
[5] S.M. Arifuzzaman, S. Rohani, Experimental study of brushite precipitation, Journal of Crystal Growth 267 (2004) 624–634.
[6] M. Bohner, Calcium orthophosphates in medicine: from ceramics to calcium phosphate cements, Injury 31 (2000) 37–47.
[7] J. Lu, M. Descamps, J. Dejou, G. Koubi, P. Hardouin, J. Lemaitre, J.P. Proust, The biodegradation mechanism of calcium phosphate biomaterials in bone, Journal of Biomedical Materials Research 63 (2002) 408–412.
[8] F. Theiss, D. Apelt, B. Brand, A. Kutter, K. Zlinszky, M. Bohner, S. Matter, C. Frei, J.A. Auer, B. von Rechenberg, Biocompatibility and resorption of a brushite calcium phosphate cement, Biomaterials 26 (2005) 4383–4394.
[9] L.M. Grover, J.C. Knowles, G.J.P. Fleming, J.E. Barralet, In vitro dissolution of brushite cement, Biomaterials 24 (2003) 4133–4141.
[10] G. Penel, N. Leroy, P. Van Landuyt, B. Flautre, P. Hardouin, J. Lemaitre, G. Leroy, Raman microspectrometry studies of brushite cement: in vivo evaluation in a sheep model, Bone 25 (1999) 81–84.
[11] P. Fraysinnet, L. Gineste, P. Conte, J. Fages, N. Rouquet, Short term implantation effects of a DCPD based calcium phosphate cement, Biomaterials 19 (1998) 971–977.
[12] B.R. Constantz, B.M. Barr, I.C. Ison, M.T. Fulmer, J. Baker, L. McKinney, S.B. Goodman, S. Gunasekaren, D.C. Delaney, J. Ross, R.D. Poser, Histological, chemical, and crystallographic analysis of four calcium phosphate cements in different rabbit osseus sites, Journal of Biomedical Materials Research 43 (1998) 451–461.
[13] M. Vallet-Regi, J.M. Gonzalez-Calbet, Calcium phosphates as substitution of bone tissues, Progress in Solid State Chemistry 32 (2004) 1–31.
[14] X. Dai, S. Shivkumar, Hybrid analogs for the production of porous calcium phosphate scaffolds, Materials Science and Engineering C 28 (2008) 336–340.
[15] H.C. Hsu, C.Y. Chiu, W.H. Tuan, H.Y. Lee, Structural stability of calcium phosphate cement during aging in water, Materials Science and Engineering C 28 (2008) 429–433.
[16] S. Singh, P. Bhardwaj, V. Singh, S. Aggarwal, U.K. Mandal, Synthesis of nanocrytalline calcium phosphate in microemulsion-effect of nature of surfactants, Journal of Colloid and Interface Science 319 (2008) 322–329.
[17] W. Paul, C.P. Sharma, Development of porous spherical hydroxyapatite granules: application towards protein delivery, Journal of Materials Science 10 (1999) 383–388.
[18] M. Jarcho, Calcium phosphate ceramics as hard tissue prosthesis, Clinical Orthopaedics and Related Research 157 (1981) 259–278.
[19] M. Jarcho, J.F. Kay, K.I. Gumaer, R.H. Doremus, H.P. Drobeck, Tissue, cellular and subcellular events at a bone-ceramic hydroxylapatite interface, Journal of Bioengineering 1 (1977) 79–92.
[20] J.W. Frame, C.L. Brady, Augmentation of an atrophic edentulous mandible by interpositional grafting with hydroxylapatite, Journal of Oral and Maxillofacial Surgery 42 (1984) 89–92.
[21] American Dental Association Council on Dental Materials, Instruments and Equipment, Council on Dental Research, Council on Dental Therapeutics, Hydroxylapatite, beta tricalcium phosphate, and autogenous and allogeneic bone for filling periodontal defects, alveolar ridge augmentation, and pulp capping, Journal of the American Dental Association 108 (1984) 822–827.
[22] J.N. Kent, M.F. Zide, J.F. Kay, M. Jarcho, Hydroxyapatite blocks and particles as bone graft substitutes in orthognathic and reconstructive surgery, Journal of Oral and Maxillofacial Surgery 44 (1986) 597–605.
[23] J. Fan, J. Lei, C. Yu, B. Tu, D. Zhao, Hard templating synthesis of a novel rod-like nanoporous calcium phosphate bioceramics and their capacity as antibiotic carriers, Materials Chemistry and Physics 103 (2007) 489–493.

[24] Y.J. Wang, C. Lai, K. Wei, S.Q. Tang, Influence of temperature, ripening time, and cosurfactant on solvothermal synthesis of calcium phosphate nanobelts, Materials Letters 59 (2005) 1098–1104.
[25] X.D. Kong, X.D. Sun, J.B. Lu, F.Z. Cui, Mineralization of calcium phosphate in reverse microemulsion, Current Applied Physics 5 (2005) 519–521.
[26] Y.J. Zhan, C.L. Zheng, Y.K. Liu, G.H. Wang, Synthesis of NiO nanowires by an oxidation route, Materials Letters 57 (2003) 3265–3268.
[27] J.D. Hopwood, S. Mann, Synthesis of barium sulfate nanoparticles and nanofilaments in reverse micelles and microemulsions, Chemistry of Materials 9 (1997) 1819–1828.
[28] C.S. Liu, W. Gai, S.H. Pan, Z.S. Liu, The exothermal behavior in the hydration process of calcium phosphate cement, Biomaterials 24 (2003) 2995–3003.
[29] K.L. Yadav, P.W. Brown, Formation of hydroxyapatite in water, Hank's solution, and serum at physiological temperature, Journal of Biomedical Materials Research 65A (2003) 158–163.
[30] Y. Wang, S. Zhang, K. Wei, N. Zhao, J. Chen, X. Wang, Hydrothermal synthesis of hydroxyapatite nanopowders using cationic surfactant as a template, Materials Letters 60 (2006) 1484–1487.
[31] Y. Xu, D. Wang, L. Yang, H. Tang, Hydrothermal conversion of coral into hydroxyapatite, Materials Characterization 47 (2001) 83–87.
[32] G.K. Lim, J. Wang, S.C. Ng, C.H. Chew, L.M. Gan, Processing and hydroxyapatite via microemulsion and emulsion routes, Biomaterials 18 (1997) 1433–1439.
[33] K. Sonoda, T. Furuzono, D. Walsh, K. Sato, J. Tanaka, Influence of emulsion on crystal growth of hydroxyapatite, Solid State Ionics 151 (2002) 321–327.
[34] J.H. Fendler, Atomic and molecular clusters in membrane mimetic chemistry, Chemical Reviews 87 (1987) 877–899.
[35] B.K. Paul, S.P. Moulik, Microemulsions: an overview, Journal of Dispersion Science and Technology 18 (1997) 301–367.
[36] N.M. Huang, S. Radiman, H.N. Lim, S.K. Yeong, P.S. Khiew, W.S. Chiu, S.N. Kong, G.H.M. Saeed, Synthesis and characterization of ultra small PbS nanorods in sucrose ester microemulsion, Materials Letters 63 (2009) 500–503.
[37] G.S. Guo, Y.X. Sun, Z.H. Wang, H.Y. Guo, Preparation of hydroxyapatite nanoparticles by reverse microemulsion, Ceramics International 31 (2009) 869–872.
[38] C. Lai, S.Q. Tang, Y.J. Wang, K. Wei, Formation of calcium phosphate nanoparticles in reverse microemulsions, Materials Letters 59 (2005) 210–214.
[39] Y. Wu, S. Bose, Nanocrystalline hydroxyapatite: micelle templated synthesis and characterization, Langmuir 21 (2005) 3232–3234.
[40] JCPDS PDF-2, ICDD Newtown Square, PA, 2001.
[41] R. Boistelle, I. Lopez-Velero, Growth units and nucleation: the case of calcium phosphates, Journal of Crystal Growth 102 (1990) 609–617.
[42] F. Abbona, H.E.L. Madsen, R. Boistelle, The initial phases of calcium and magnesium phosphates precipitated from solutions of high to medium concentrations, Journal of Crystal Growth 74 (1986) 581–590.
[43] J.C. Elliott, Structure and Chemistry of the Apatites and Other Calcium Orthophosphates, Elsevier, Amsterdam, 1994.
[44] H.E.L. Madsen, F. Christensson, Precipitation of calcium phosphate at 40 °C from neutral solution, Journal of Crystal Growth 114 (1991) 613–618.
[45] A. Ferreira, C. Oliveira, F. Rocha, The different phases in the precipitation of dicalcium phosphate dihydrate, Journal of Crystal Growth 252 (2003) 599–611.
[46] O. Glatter, D. Orthaber, A. Stradner, G. Scherf, M. Fanun, N. Garti, V. Clement, M.E. Leser, Sugar-ester nonionic microemulsion: structural characterization, Journal of Colloid and Interface Science 241 (2001) 215–225.
[47] X. Lu, Y. Wang, J. Wang, S. Qu, J. Weng, R. Xin, Y. Leng, Calcium phosphate crystal growth under controlled environment through urea hydrolysis, Journal of Crystal Growth 297 (2006) 396–402.
[48] L.F. Xi, Y.M. Lam, Synthesis and characterization of CdSe nanorods using a novel microemulsion method at moderate temperature, Journal of Colloid and Interface Science 316 (2007) 771–778.
[49] M.P. Pileni, Reverse micelles used as templates: a new understanding in the nanocrystal growth of silver and copper nanocrystals by using hydrazine as reducing agent, Journal of Experimental Nanoscience 1 (2006) 13–27.
[50] Z.A. Peng, X.G. Peng, Nearly monodisperse and shape-controlled CdSe nanocrystals via alternative routes: nucleation and growth, Journal of the American Chemical Society 124 (2002) 3343–3353.
[51] M.P. Pileni, Water-in-oil colloidal droplets used as microreactors, Advances in Colloid and Interface Science 46 (1993) 139–163.